

A semi-analytical method for quantifying the size-dependent elasticity of nanostructures

Rémi Dingreville, Ambarish J Kulkarni, Min Zhou and Jianmin Qu

G. W. Woodruff School of Mechanical Engineering, Georgia Institute of Technology, Atlanta, GA 30332-0405, USA

Received 16 July 2007, in final form 30 November 2007

Published 11 January 2008

Online at stacks.iop.org/MSMSE/16/025002

Abstract

In this paper, a semi-analytical method is developed to compute the elastic stiffness of nanostructures such as nanowires, nanotubes and nanofilms. Compared with existing methods for such computations, this new method is more accurate and significantly reduces the computational time. It is based on the Taylor series expansion of an interatomic potential about the relaxed state of a nanostructure and implicitly accounts for the effects of shape, size and surface of the nanostructures. To analyze the applicability and accuracy of this method, as a case study, calculations are carried out to quantify the size dependence of the elastic moduli of nanofilms and nanowires with [001], [110] and [111] crystallographic growth orientations for groups 10 and 11 transition metals (Cu, Ni, Pd and Ag). The results are in excellent agreement with data in the literature and reveal consistent trends among the materials analyzed.

1. Introduction

Nanostructures such as nanowires, nanotubes and nanofilms exhibit unique mechanical, electronic, optical and magnetic properties [1, 2] that do not exist in the case of classical bulk structures. These nanostructured materials can play a major role in nanoelectromechanical (NEMS) devices. The dependence of the thermo-mechanical responses of such nanostructures on size is one unique aspect of their behavior [3–13]. The difference in behavior between bulk structures and nanostructures stems partly from the large surface-to-volume ratio at the nanoscale and therefore the effects of surfaces can no longer be neglected when the overall behavior of these nanostructures is considered [1, 2, 14]. This size dependence at the nanoscale represents both a challenge and an opportunity to regulate their properties for device integration. The study and characterization of the mechanical behavior and the effective properties of nanostructures are therefore important for the development of nanomaterials and for the design of devices that utilize such nanostructures.

A variety of atomistic simulation methods have been used to study the effective elastic properties of nanostructural elements. Based on density functional theory (DFT), first

principles methods have been used to directly calculate the material properties of nanostructures [15–17]. These calculations provide a deeper understanding of the physics by considering the electronic structures of small clusters of atoms. Unfortunately, they are limited to the study of small systems since the computational time associated with larger systems of atoms is prohibitively long. On the other hand, molecular dynamics (MD) calculations allow for the study of reasonably large systems and have been used as an alternative to *ab initio* calculations. For example, MD simulations have been widely used to study the deformation mechanisms of nanostructures [18–21]. The deformation analyses involve both quasi-static and dynamic conditions. In the case of dynamic loading, it is often necessary to apply extremely high-strain rates (on the order of 10^9 s^{-1}) in order to reach strain levels of practical interest using existing computers. However, such high-strain rates can alter the response of the material and introduce variability in the characterization of the elastic constants. In the quasi-static framework, deformations are achieved through a sequence of strain and relaxation steps that circumvent the need for high-strain rate loading and its related problems. But computation is still limited by the computational time required to relax the structure after each strain increment. Furthermore, in both types of approaches (dynamic and quasi-static), the effective elastic moduli are computed from the stress–strain curves obtained from the simulations. Therefore, multiple simulations and different loading modes are required to obtain all elastic constants. For highly anisotropic materials, these methods are tedious and lengthy. Additionally, computing the slopes of the numerically interpolated stress–strain curves often leads to unacceptable levels of error.

Molecular statics (MS) represents another family of computational techniques used to study the mechanical response of nanostructures. For example, Liang *et al* [22] employed an MS approach to study the size-dependent elastic behavior of copper nanowires along the [0 0 1], [1 1 0] and [1 1 1] crystallographic directions. They performed a strain meshing of the nanostructure followed by an energy minimization for each deformation step. Subsequently, the elastic constants are obtained by numerical interpolation of the energy density meshing in the strain space. This method is also very tedious and time consuming since a refined strain mesh is necessary in order to obtain accurate results. Another example of quasi-static MS calculations consisting of applying a uniform uniaxial strain incrementally to the relaxed nanowire configurations followed by energy minimization was employed by Diao and coworkers [4] to study the effect of free surfaces and edges on the structure and elastic properties of gold nanowires aligned in the [1 0 0] and [1 1 1] directions. For the particular case of FCC metal nanowires considered in their work, this method requires moderate computational resources. However, this method can be computationally demanding in studying inorganic compound materials where the calculation of electrostatic contributions to the total energy is computationally inefficient for nanostructures (for example, ZnO and GaN nanowires). Another drawback of this method is that it can only evaluate elastic properties at 0 K.

As an alternative to the atomistic simulations, various approaches have also been developed to extend continuum theories to nanostructured materials in order to incorporate surface structure and its effects in the evaluation of the overall behavior of nanostructures [12, 23–25]. Specifically, several available thermodynamic models allow the size dependence of the elastic response of nanostructures to be characterized through the inclusion of surface free energy or surface stresses. In particular, using harmonic potentials and springs in a semi-continuum model, Sun [24] predicted a decrease in the elastic modulus with the thickness of thin films. Zhang [25] developed a theory linking interatomic potentials and the atomic structure of a material to a constitutive model at the continuum level and applied it to the study of the linear elastic modulus of single-wall carbon nanotubes. Dingreville *et al* [26] developed a general framework for incorporating surface free energy into the continuum representation of mechanical behavior. Based on this approach, they demonstrated that the overall elastic

behavior of structural elements (such as particles, wires and films) is size dependent and observed that the self-equilibrium state of a particle is different from that of an infinite crystal lattice and attributed the difference primarily to the effect of surface stresses. These methods prove to be powerful analytical tools and give a deeper insight of the physical phenomenon associated with nanostructures. Nevertheless, they require the knowledge of the material properties such as bulk and surface elastic constants, which, in turn, generally necessitate atomistic calculations for their evaluation. Many approaches have been developed to experimentally measure [27, 28] or computationally evaluate the required surface properties such as surface energy, surface stress and surface stiffness. In particular, first principles, MD and MS calculations have been used, often along with analytical or semi-analytical models. For example, as early as 1986 Ackland and Finnis [29] calculated the tensile surface stresses in body-centered cubic (BCC) and face-centered cubic (FCC) metals using simple empirical N-body potentials. Their result was in satisfactory agreement with available experimental data. Later on, researchers such as Daw and co-workers [30–32], or Mishin and coworkers [33–35], successfully evaluated the ability of the embedded-atom method (EAM) potentials to predict energies and stability of non-equilibrium structures. Recently, Dingreville and Qu [36] developed a semi-analytical method and successfully used it to compute the intrinsic surface energy density, intrinsic surface stress and surface stiffness of crystalline materials. In addition to these prerequisites, the implementations of these analytical methods can be complicated when dealing with nanostructures having more complex shapes than wires and thin films.

In summary, most of the existing methods for computing the elastic properties of nanostructural elements are rather complicated to implement and are computationally intensive. The semi-analytical method proposed in this work overcomes most of the aforementioned disadvantages. This approach allows the effective elastic properties of nanostructures to be expressed analytically in terms of the interatomic potential of the material and the equilibrium (or relaxed) positions of the atoms. Once the initial assembly is created and equilibrated no further atomistic simulations are necessary in order to obtain the elastic properties. This method is written in a general form so that, firstly, it admits a generic interatomic potential and, therefore, it can be used for a wide range of materials and, secondly, the effects of the size and shape of the nanostructure are implicitly considered through the equilibrated geometry of the nanostructure. Compared with the existing methods, the method presented here significantly reduces the computational time (94% reduction as compared with the MD/MS simulation schemes detailed above) since it only requires one static relaxation calculation. It also avoids potential sources of errors in the results obtained by directly computing the elastic constants and obviating any numerical interpolation or thermodynamics ensemble averaging.

In what follows, we first derive the analytical expressions for effective elastic properties and extend the methodology to the characterization of the size dependence of the elastic moduli of thin films and nanowires grown along the [00 1], [1 1 0] and [1 1 1] crystallographic directions for group 10–11 transition metals (Cu, Ni, Pd and Ag) using EAM potentials.

2. Method for computing the effective elastic constants of nanostructures

This section outlines the semi-analytical method for evaluating the effective elastic properties of nanostructures measured at the relaxed configuration. The interatomic potential and the computational framework used in the application of this method to nanowires and nanofilms are also discussed.

2.1. Derivation of the method

A generic interatomic potential function $E^{(n)}$ for atom n in its self-equilibrium position of a crystalline material can be written as

$$E^{(n)} = E_0 + \sum_{m \neq n} E_1(\hat{r}^{nm}) + \frac{1}{2!} \sum_{m \neq n} \sum_{p \neq n} E_2(\hat{r}^{nm}, \hat{r}^{np}) + \dots + \frac{1}{N!} \sum_{m \neq n} \sum_{p \neq n} \dots \sum_{q \neq n} E_N(\hat{r}^{nm}, \hat{r}^{np}, \dots, \hat{r}^{nq}), \quad (1)$$

where

$$\hat{r}^{mn} = \sqrt{(\hat{r}_1^{mn})^2 + (\hat{r}_2^{mn})^2 + (\hat{r}_3^{mn})^2} \quad (2)$$

is the scalar distance between atoms m and n in the relaxed configuration. Note that the generic form in equation (1) includes pair potentials such as the Lennard-Jones potential as well as multi-body potentials such as the EAM potential used in the numerical examples in this paper. The vector \mathbf{r}^{mn} is the position vector between atoms m and n in a uniform strain field measured from the relaxed configuration of the nanostructure. The strain tensor relative to the relaxed configuration here is assumed to be the same for all atoms and can be defined through

$$\mathbf{r}^{mn} - \hat{\mathbf{r}}^{mn} = \tilde{\eta}_{ij}^{mn} \hat{r}_j^{mn} = \tilde{\eta}_{ij} \hat{r}_j^{mn}. \quad (3)$$

Additional deformation for atoms near the surfaces is therefore assumed to be uniform when the nanostructure is subsequently deformed from its relaxed state. The nine independent components of the deformation gradient $\tilde{\eta}_{ij}$ can now be decomposed into six symmetric parameters corresponding to the pure deformation

$$\tilde{\varepsilon}_{ij} = \frac{1}{2}(\tilde{\eta}_{ij} + \tilde{\eta}_{ji}) \quad (4)$$

and three anti-symmetric parameters corresponding to the pure rotation

$$\gamma_{ij} = \frac{1}{2}(\tilde{\eta}_{ij} - \tilde{\eta}_{ji}). \quad (5)$$

In this work, only the pure deformation $\tilde{\varepsilon}_{ij}$ is considered and the rotation γ_{ij} is neglected in the formulation since only axial behaviors are considered here. It then follows from the previous work by Johnson [37, 38] that, for a uniform and homogeneous deformation, the Taylor expansion of (1) with respect to the relaxed configuration can be written as

$$E^{(n)} = A^{(n)} + A_{ij}^{(n)} \tilde{\varepsilon}_{ij} + \frac{1}{2} A_{ijkl}^{(n)} \tilde{\varepsilon}_{ij} \tilde{\varepsilon}_{kl}, \quad (6)$$

where the uniform strain field $\tilde{\varepsilon}_{ij}$ is measured from the equilibrium (relaxed) state of the nanostructure and the coefficients $A^{(n)}$, $A_{ij}^{(n)}$ and $A_{ijkl}^{(n)}$ are related to the energy of atom n via

$$A^{(n)} = E^{(n)}|_{r^{mn}=\hat{r}^{mn}}, \quad (7)$$

$$A_{ij}^{(n)} = \left[\sum_{p \neq n} \hat{r}_i^{pn} \frac{\partial E^{(n)}}{\partial r_j^{pn}} \right]_{r^{mn}=\hat{r}^{mn}} \Big|_{(i,j)} \quad (8)$$

and

$$A_{ijkl}^{(n)} = \left[\sum_{p \neq n} \sum_{q \neq n} \frac{\hat{r}_i^{pn} \hat{r}_k^{qn} \partial^2 E^{(n)}}{\partial r_j^{pn} \partial r_l^{qn}} \right]_{r^{mn}=\hat{r}^{mn}} \Big|_{(i,j),(k,l)}. \quad (9)$$

Here, the symbol $\langle i, j \rangle$ in the subscript indicates the symmetric part of the base tensor, i.e.

$$[u_{i,j}]_{(i,j)} = \frac{1}{2}[u_{i,j} + u_{j,i}]. \quad (10)$$

Note that, once the interatomic potential $E^{(n)}$ is given and the relaxed (equilibrium) position of each atom in the system is known, the coefficients $A^{(n)}$, $A_{ij}^{(n)}$ and $A_{ijkl}^{(n)}$ can be computed analytically.

For any given atom belonging to the nanostructure (either on the surface or in the core), the local elastic stiffness tensor can then be defined as

$$C_{ijkl}^{(n)} = \frac{1}{\Omega^{(n)}} A_{ijkl}^{(n)}, \quad (11)$$

where $\Omega^{(n)}$ is the volume of the Voronoi polyhedron associated with atom n . The atomic-level elastic stiffness tensor $C_{ijkl}^{(n)}$ can be interpreted as a description of the homogeneous elastic response at individual atomic sites. We can now consider the entire structure with volume Ω that contains N atoms. When subjected to a uniform strain field ε_{ij} , the elastic stiffness tensor of the nanostructure measured at the relaxed state is thus given by

$$C_{ijkl} = \frac{1}{N} \sum_{n=1}^N \frac{1}{\Omega_n} A_{ijkl}^{(n)} = \frac{1}{N} \sum_{n=1}^N \sum_{p \neq n} \sum_{q \neq n} \frac{1}{\Omega_n} \left. \frac{\hat{r}_j^{pn} \hat{r}_l^{qn} \partial^2 E_n(r^{mn})}{\partial r_i^{pn} \partial r_k^{qn}} \right|_{r^{mn} = \hat{r}^{mn}}. \quad (12)$$

Note that under the above assumptions, this formula generally gives analytical expressions of the Voigt upper bound of the effective stiffness tensor of the nanostructure considered at the state of self-equilibrium. In the particular situation of thin films and nanowires grown along the basal crystallographic directions, as is the case in this paper, it has been verified that the transverse relaxation is linear and therefore the above equation gives the exact expression of the effective stiffness tensor of the nanostructure considered at the state of self-equilibrium.

In the particular case of nanowires, it is convenient to consider the uniaxial elastic modulus defined as

$$E_{X_3} = E_L = C_{33} + \frac{C_{11}C_{23}^2 + C_{22}C_{13}^2 - 2C_{12}C_{13}C_{23}}{C_{12}^2 - C_{11}C_{22}}, \quad (13)$$

where C_{ij} are the contracted forms of the effective stiffness tensor C_{ijkl} under the Voigt notations. The general rule for contracting the indices is (11) \rightarrow (1), (22) \rightarrow (2), (33) \rightarrow (3), (12) \rightarrow (6), (13) \rightarrow (5), (23) \rightarrow (4). For example, $C_{1122} = C_{12}$.

Similarly, for thin films, quantities of interest are the two in-plane unidirectional elastic moduli

$$E_{X_1} = E_1 = C_{11} + \frac{C_{33}C_{12}^2 + C_{22}C_{13}^2 - 2C_{12}C_{13}C_{23}}{C_{23}^2 - C_{22}C_{33}}, \quad (14)$$

$$E_{X_2} = E_2 = C_{22} + \frac{C_{33}C_{12}^2 + C_{11}C_{23}^2 - 2C_{12}C_{13}C_{23}}{C_{13}^2 - C_{11}C_{33}} \quad (15)$$

and the biaxial elastic modulus

$$Y = \frac{1}{2} \left[C_{11} + C_{22} + 2C_{12} - \frac{(C_{13} + C_{23})^2}{C_{33}} \right]. \quad (16)$$

Note that the elastic constants are defined with respect to the relaxed configuration of the nanostructures. The method described here is not limited to wires and films. It can be used to deal with nanostructures of more complex shapes and sizes. Obviously, this approach implicitly accounts for the surface effects that influence the properties of the structure. It is therefore important to choose an appropriate interatomic potential function in order to have an accurate description of the properties of the material studied.

2.2. Interatomic potential

The formulation developed here is very general in the sense that it applies to any interatomic potential as long as a functional form for the potential exists. However, it should be noted that the predictions of this method are as accurate as the potential itself, as is the case with all the methods outlined above. We have used an EAM potential developed by Daw and Baskes [31, 32] as a study case in this paper for numerical evaluation since it is a very efficient technique for modeling realistic metallic cohesion [31, 32, 39]. Furthermore, for nanostructures, the physical nature of the surface atoms is different from that in the bulk, and deviations from the bulk elastic behavior in small scale systems can be considered as manifestations of the Gibbs–Thomson effect. It has been shown in a previous paper by the authors [36] that the EAM potential used in this work adequately predicts surface properties such as surface energy and surface stress. Hence, it ensures that surface properties are being modeled correctly so that their influences on small sized solids are appropriately taken into account when determining the effect of surfaces on the elastic properties. This many-body potential also has the advantage [40] of keeping the computations scaling on the order of N whereas more complex many-body potentials are on the order of N^3 which renders the numerical interpolation of the potential lengthier.

In this framework, the total energy of an atom is expressed as the sum of contributions from the two-body interactions and from an embedding energy, i.e.

$$E_n = E_n^G + E_n^V = G_n(\bar{\rho}_n) + \frac{1}{2} \sum_{m \neq n} V(r^{mn}), \quad (17)$$

where E_n^G and E_n^V represent, respectively, the embedding energy of atom n and the pair interaction potential between atoms m and n . $\bar{\rho}_n$ is the local background electron density induced at the position of atom n by other atoms in the system calculated as a linear superposition of the contributions from those atoms. These functions have been determined empirically by fitting the predicted results to experimental values or values obtained using *ab initio* techniques. These include physical properties such as the equilibrium lattice parameter, cohesive energy, sublimation energy, elastic constants C_{11} , C_{12} and C_{44} and vacancy-formation energy. The explicit expressions of equations (7)–(9) for the EAM potentials used are derived in the appendix.

In this paper, the contribution of kinetic energy or temperature is neglected. The free energy involves contributions from both the internal energy of the crystal and the product of the entropy and absolute temperature. The latter contribution vanishes at 0 K. The atomic rearrangements are regular and smooth enough such that the configurational and thermal sources of entropy can be ignored. In fact, it has been proven that in the case of nanowires and thin films the elastic modulus decreases approximately linearly with increasing temperature [41, 42], with a decrease of up to 15% over a temperature range of 0–400 K for copper, for example. Therefore, the internal energy at 0 K constitutes a fair measure [43] of the elastic modulus at low temperatures and can be simply interpolated to a finite temperature by a linear regression. The evaluation of the elastic modulus at a higher temperature could be achieved by computing the relaxed state of the structure at the desired temperature and subsequently used the proposed method in this paper to calculate its effective stiffness.

2.3. Computational framework

The framework developed earlier is used to study the size dependence of the effective elastic constants of [1 0 0]-, [1 1 0]- and [1 1 1]-oriented FCC nanofilms and nanowires with square cross sections of groups 10–11 transition metals. Figure 1 shows the orientations of the lateral

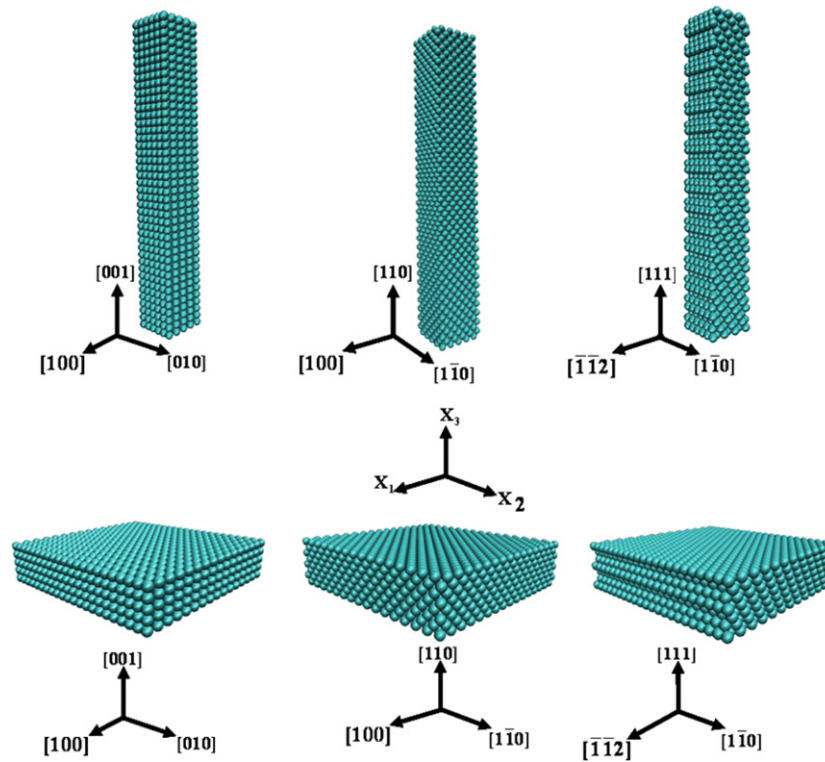


Figure 1. Schematic illustration of the nanostructural elements analyzed and their crystallographic orientations. PBCs are applied in the longitudinal directions (X_3 axis in the case of nanowires, X_1 and X_2 axes in the case of nanofilms). The transversal directions are kept traction free. (This figure is in colour only in the electronic version)

surfaces of these nanostructures. The full set of effective elastic constants for Cu, Ni, Ag and Pd nanowires and thin films are calculated.

Nanostructures of different sizes are obtained by considering a top down fabrication approach [44] by ‘cutting’ them from bulk crystals in the desired crystallographic orientations. Periodic boundary conditions (PBCs) are applied along the longitudinal direction and the lateral surfaces are kept free. For nanowires, PBCs are applied along the X_3 axis, as illustrated in figure 1. For nanofilms, PBCs are applied in the X_1 and X_2 directions. It is found that computational cell lengths of at least 6 nm for wires and in-plane widths of at least 4 nm for films are needed to ensure that the results are independent of the choices of computational cell sizes. Therefore, a cell length of 20 nm is used for all the nanowires and a cross-sectional size of 8 nm \times 8 nm is used for all films.

The atomic interactions are calculated up to the third nearest neighbor by truncating the EAM potential at the appropriate distance. The reduced coordination of atoms near free surfaces induces a redistribution of electronic charges which alters the binding situation. Consequently, atoms near surfaces relax or move away from their perfect lattice positions and, as a result, their energy is different from the values in bulk. A non-linear conjugate gradient method is used to minimize the energy of the system and to obtain the relaxed configuration. Contractions in the longitudinal and transverse directions are observed upon relaxation. This self-equilibrium state is characterized by the relaxation-induced strain field $\hat{\epsilon}_{ij}$ and the average

stress over the entire structure which is equal to zero since the structure is in a free-standing state.

The effective elastic moduli of thin films and wires of various thicknesses obtained from the semi-analytical model (labeled as ‘*atomistic*’ in subsequent graphs) were compared with those calculated using a continuum model developed by Dingreville *et al* [26] (labeled as ‘*model*’ in subsequent graphs). This continuum model proves to give accurate estimations of the elastic constants of diverse nanostructures and compares well with other existing techniques evaluating those constants. In this continuum model, the relaxed state of the nanostructure is characterized by the strain tensor, $\hat{\epsilon}_{ij}$, that describes the deformation from the perfect crystal lattice to the self-equilibrium state of the particle and can be analytically written as

$$\hat{\epsilon}_{ij} = -\frac{1}{d} M_{ijkl} \tau_{kl}, \quad (18)$$

where $M_{ijkl} = C_{ijkl}^{-1}$ is the compliance tensor of the bulk crystal, τ_{ij} is the intrinsic surface stress tensor and d is the characteristic length of the particle. The effective modulus tensor of the particle evaluated at the state of self-equilibrium was expressed as

$$\bar{C}_{ijkl} = C_{ijkl}^+ \frac{1}{a} (Q_{ijkl} - C_{ijklmn}^{(3)} M_{mnpq} \tau_{pq}). \quad (19)$$

The fourth order tensor Q_{ijkl} can be viewed as a surface rigidity tensor. It represents the combined effect of surface stiffness and surface geometry. $C_{ijklmn}^{(3)}$ represents the third order elastic constants of the perfect crystal lattice. These two equations were used to compare with the results obtained through the method presented in this paper.

3. Results for thin films and nanowires

Three different crystallographic orientations in four FCC materials (Cu, Ni, Ag and Pd) are considered. The discussion here focuses on the elastic properties of these homologous materials and the underlying trends in the effects of surface and crystallographic orientations. The values for cubic (second order) and third order elastic constants of the single crystals and the surface properties required for the continuum model are taken from Dingreville [36, 45] and are listed in tables 1 and 2. All the results discussed in this paper are for unreconstructed surfaces. As reported by several researchers [4, 8, 9], for certain orientations and materials, phase transformation and surface and structure reconstruction can occur when the characteristic size is sufficiently small. Examples include [1 0 0]-oriented gold nanowires with cross-sectional areas smaller than $1.83 \text{ nm} \times 1.83 \text{ nm}$. The sizes considered in this paper are larger than the critical sizes associated with the lattice reorientation phenomenon; therefore, there is no need to consider issues related to structural changes.

Figure 2 shows the self-equilibrium strains during the initial relaxation of nickel nanowires as a function of wire thickness. Results computed via equation (18) from the continuum model developed by Dingreville *et al* [26] are also shown. For the three crystallographic orientations and for all the materials studied, the self-equilibrium strains obtained from the atomistic calculations agree well with the calculated values using the continuum model. As seen from the continuum and semi-analytical model results, we observe longitudinal contractions and lateral expansions that increase as the size of the wires decreases. For a given wire size, the axial contractions for the [1 1 0] and [1 1 1] directions have similar magnitudes and they are furthermore larger than those of [1 0 0] wires. For example, for a 2 nm wire, the equilibrium strain is approximately -1% for [1 1 0] and [1 1 1] wires while it is approximately -2% for [1 0 0] wires. Table 1 shows that for all the metals studied, the intrinsic surface stresses $\Gamma_{11}^{(1)}$ and $\Gamma_{22}^{(1)}$ of the (1 0 0) surfaces are greater than the surface stresses of the two other surfaces, while

Table 1. Elastic properties of low-index surfaces of several FCC metals (obtained using the method of Dingreville and Qu [36]): unit: J m^{-2} .

		Ni	Cu	Pd	Ag
(1 1 1)	$\Gamma_{11}^{(1)}$	0.457	0.866	1.848	0.636
	$\Gamma_{1111}^{(2)}$	6.526	2.054	-2.914	0.888
	$\Gamma_{1122}^{(2)}$	3.986	1.086	-1.014	1.194
	$\Gamma_{1212}^{(2)}$	-1.188	-1.071	-2.354	-1.173
(1 0 0)	$\Gamma_{11}^{(1)}$	1.321	1.396	1.981	0.816
	$\Gamma_{1111}^{(2)}$	-0.865	-0.712	-2.360	-1.245
	$\Gamma_{1122}^{(2)}$	10.722	5.914	2.611	3.343
	$\Gamma_{1212}^{(2)}$	-0.927	-0.992	-3.250	-1.666
(1 1 0)	$\Gamma_{11}^{(1)}[001]$	1.054	1.126	1.230	0.492
	$\Gamma_{22}^{(1)}[1\bar{1}0]$	0.706	0.993	1.656	0.684
	$\Gamma_{1111}^{(2)}$	-13.031	-7.798	-4.775	-5.510
	$\Gamma_{2222}^{(2)}$	0.950	-2.263	-6.654	-2.246
	$\Gamma_{1122}^{(2)}$	-5.045	-3.600	-2.086	-2.332
	$\Gamma_{1212}^{(2)}$	-7.827	-4.436	-3.378	-3.296

Table 2. Elastic properties of FCC metals (obtained using the method of Dingreville [45]). Unit: 100 GPa.

	Ni	Cu	Pd	Ag
C_{11}	2.329 372	1.671 006	1.982 86	1.288 681
C_{12}	1.540 882	1.240 452	1.703 933	0.908 729
C_{44}	1.274 68	0.763 766	0.579 613	0.566 601
C_{111}	-10.1788	-7.374 77	-11.295	-6.630 15
C_{112}	-7.897 58	-5.757 54	-8.816 75	-4.976 39
C_{123}	2.545 034	0.322 111	-3.440 31	0.118 789
C_{144}	0.724 419	0.283 855	-0.669 12	-0.056 54
C_{155}	-9.213 24	-5.188 77	-4.622 39	-4.632 29
C_{456}	1.335 939	0.885 549	0.693 845	0.530 193

they are similar for the (1 1 1) and (1 1 0) surfaces. Due to higher moduli in the [1 1 1] and [1 1 0] directions and smaller intrinsic surface stresses on the lateral surfaces, this results in the fact that the relaxation strain is smaller for the [1 1 0] and [1 1 1] nanowires than for the [1 0 0] wires at a given thickness. Clearly, the intrinsic residual surface stresses directly influence the magnitude of the self-equilibrium strain. A similar observation is also made for the nanofilms. This observation is confirmed by equation (18) and by previously reported results by Liang *et al* [22] and Zhou and Huang [46].

The effective unidirectional and biaxial moduli for single crystal Ni wires and Cu films of various thicknesses are plotted in figures 3 and 4, respectively. For Ni wires, the axial modulus for the [1 1 0] orientation increases as the wire diameter decreases, while an opposite trend is seen for wires in the [1 0 0] orientation. For a wire size of 2 nm, the axial modulus for the [1 0 0] orientation is approximately 15% smaller than its bulk counterpart (we calculated a reduction of up to 35% compared with the bulk value in the case of 2 nm Cu nanowires), while in the case of the wire in the [1 1 0] orientation, the axial modulus for a 2 nm wire is approximately 23% higher than the value in the bulk. As seen from figure 3, as the wire size is decreased from 8 to 2 nm, the axial elastic modulus decreases by 28% for [1 0 0] wires and

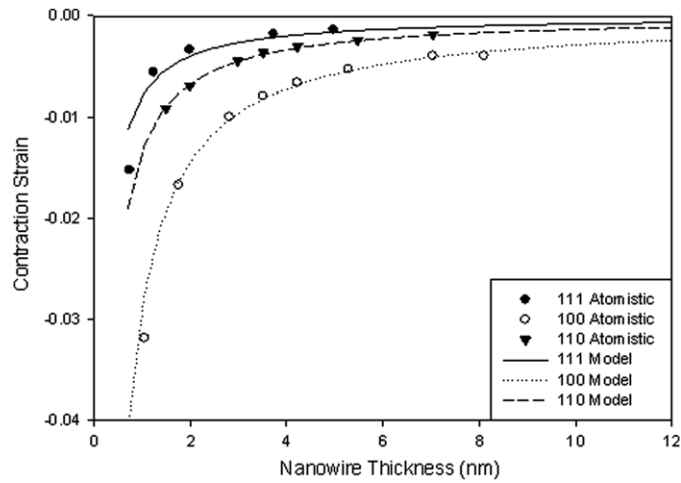


Figure 2. Self-equilibrium strain of nickel nanowires as a function of wire thickness for different crystallographic orientations calculated using the semi-analytical method (labeled as ‘atomistic’) with an EAM potential. A comparison with the results obtained using the method of Dingreville and Qu [26] (labeled as ‘model’) is also shown.

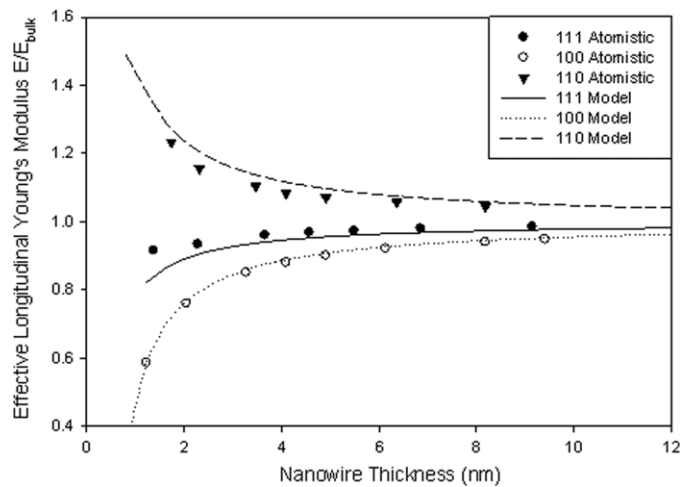


Figure 3. Effective elastic modulus in the longitudinal direction of copper nanowires as a function of wire thickness calculated using the semi-analytical method (labeled as ‘atomistic’) with an EAM potential. A comparison with the results obtained using the method of Dingreville and Qu [26] (labeled as ‘model’) is also shown.

by only 2% for [1 1 1] wires, while it increases by 15% for [1 1 0] wires. This can simply be explained through equation (19). It is clear from this expression that the two material properties influencing the softening or stiffening of nanostructures are (i) the surface elasticity represented through the tensor Q_{ijkl} (which is a function of the surface elastic behavior and the shape of the nanostructural element) and (ii) the non-linear behavior of the core of the nanostructure through the third elastic constants $C_{ijklmn}^{(3)}$. For all orientations and materials studied the surface elasticity always contributes to the softening of the wires as compared with their respective bulk values, while the non-linear elastic behavior of the core of the wire

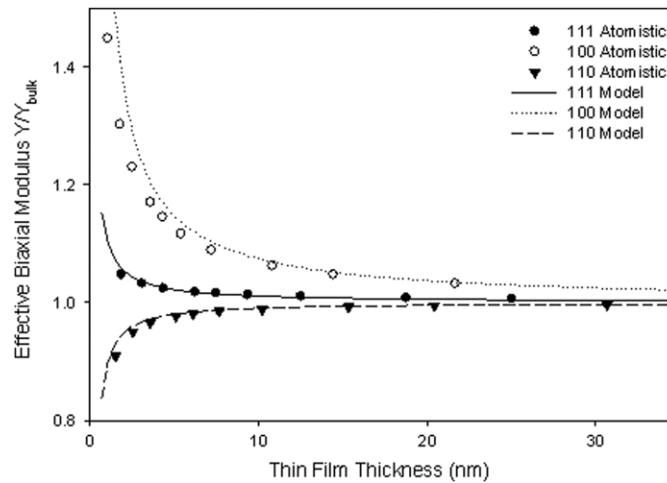


Figure 4. Effective biaxial elastic modulus of copper nanofilms as a function of film thickness calculated using the semi-analytical method (labeled as ‘atomistic’) with an EAM potential. A comparison with the results obtained using the method of Dingreville and Qu [26] (labeled as ‘model’) is also shown.

contributes to the size-dependent softening of the wire in the case of the [100] and [111] orientations and contributes to the size-dependent stiffening of the wire in the case of the [110] orientation. Similar trends are seen for the uniaxial modulus of Cu films since the films can be viewed as an array of wires placed side by side.

In the case of the biaxial elastic modulus of Cu thin films, as seen in figure 4, we observe opposite trends as compared with the uniaxial elastic modulus of the nanowires. Specifically, for a 2 nm film, the biaxial modulus for the (100) orientation is almost 33% higher than its bulk value. We can see from figure 4 that when the thickness of the film is reduced from 8 to 2 nm, the biaxial elastic modulus increases by 22% and 4% with respect to its bulk value for the (100) and (111) films, respectively, while it decreases by 4% for the (110) wires. Similar results and trends obtained by MS calculations and strain meshing are confirmed by earlier works of Liang *et al* [22] and Zhou and Huang [46].

Another interesting observation is the similarity between the size dependences of the uniaxial elastic modulus for nanowires in the [100] direction and the uniaxial elastic modulus in the (001) direction of the [110] films (figure 5). This can be qualitatively explained by considering the surface attributes for the (110) plane. In particular, the trough and ridge structure of the (110) surface results in atoms along the rows of atoms along the [110] direction being separated by a relatively wide trough. The nearest neighbors of the atoms in a row are other atoms in the same row and atoms in the layers underneath it. The only nearest neighbor bonds of the surface layers atoms that have a component transverse to the [110] row are those that connect them to the atoms in the second layer resulting in a higher uniaxial elastic modulus in the [110] direction than in the [100].

It is also interesting to note the similarity of the size dependence of the elastic response of nanocrystalline materials with the nanoparticles studied in this paper by the same order of magnitude. Indeed, previous works, both experimental [47–49] and computational [50–53], showed that the effective modulus of polycrystalline materials is also inversely proportional to the grain size. For example, some works reported a reduction in the elastic modulus by as much as 30% [49,54] for nanocrystalline materials. Careful molecular dynamic simulations of copper polycrystal [53] have shown that Young’s modulus is indeed reduced by over 25% when

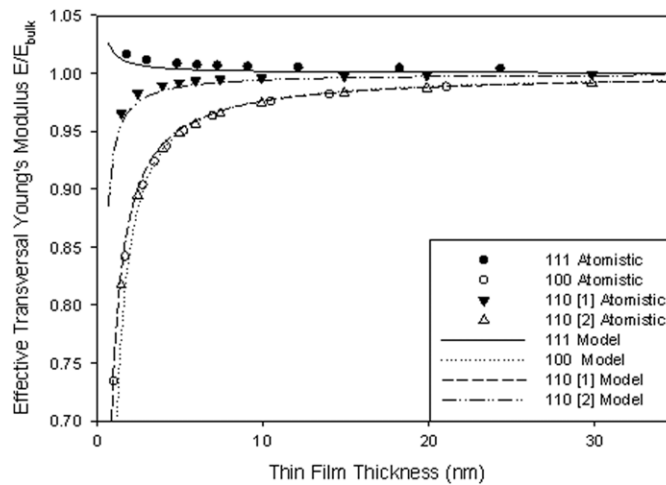


Figure 5. Effective uniaxial elastic modulus of nickel nanofilms as a function of the film thickness calculated using the semi-analytical method (labeled as ‘atomistic’) with an EAM potential. A comparison with the results obtained using the method of Dingreville and Qu [26] (labeled as ‘model’) is also shown.

the grain size is reduced to 5 nm, even when the polycrystal is fully dense. A similar reduction is seen in simulations for other materials [50,52]. It is therefore perfectly admissible to consider that the present method could capture the size dependence of nanocrystalline materials.

Before closing this section, we show in figure 6 the results for all the materials studied and compare the uniaxial elastic modulus for nanowires and uniaxial and biaxial elastic moduli for thin films as a function of their characteristic sizes. The elastic moduli decreases for the [100] wires, increases for the [110] wires and remains essentially constant for the [111] wires as the cross-sectional size is decreased (figure 6(a)). For thin films (figure 6(b)), the biaxial elastic modulus shows exactly the opposite trend to those seen in the nanowires for all the materials studied. The size dependence trends observed for the uniaxial moduli of thin films grown in various orientations are also consistent among the materials analyzed. Such a consistency in the elastic response is expected since the surface and bulk properties are quite similar for the materials in this homologous series. It is worth mentioning that, among the transition metals studied, palladium is the material most susceptible to being affected by the size dependence at the nanoscale. Although discussions on the effect of size on the unusual mechanical properties of metal nanowires have previously been reported [3, 4, 22, 46], it is believed that such a complete set of elastic properties’ data for this variety of materials is new to the literature.

4. Conclusions

A semi-analytical method for computing the elastic properties of nanostructural elements has been developed. This method is semi-analytical in that it expresses the elastic properties explicitly in terms of the interatomic potential. It requires only one MS calculation to obtain the self-equilibrium state (relaxed state) of the nanostructural elements. Compared with existing methods, this method has several advantages including (i) it does not require extensive computational resources (only one MS calculation and therefore $\sim 90\%$ reduction in the CPU time as compared with full atomistic techniques), (ii) it directly gives the full set of elastic

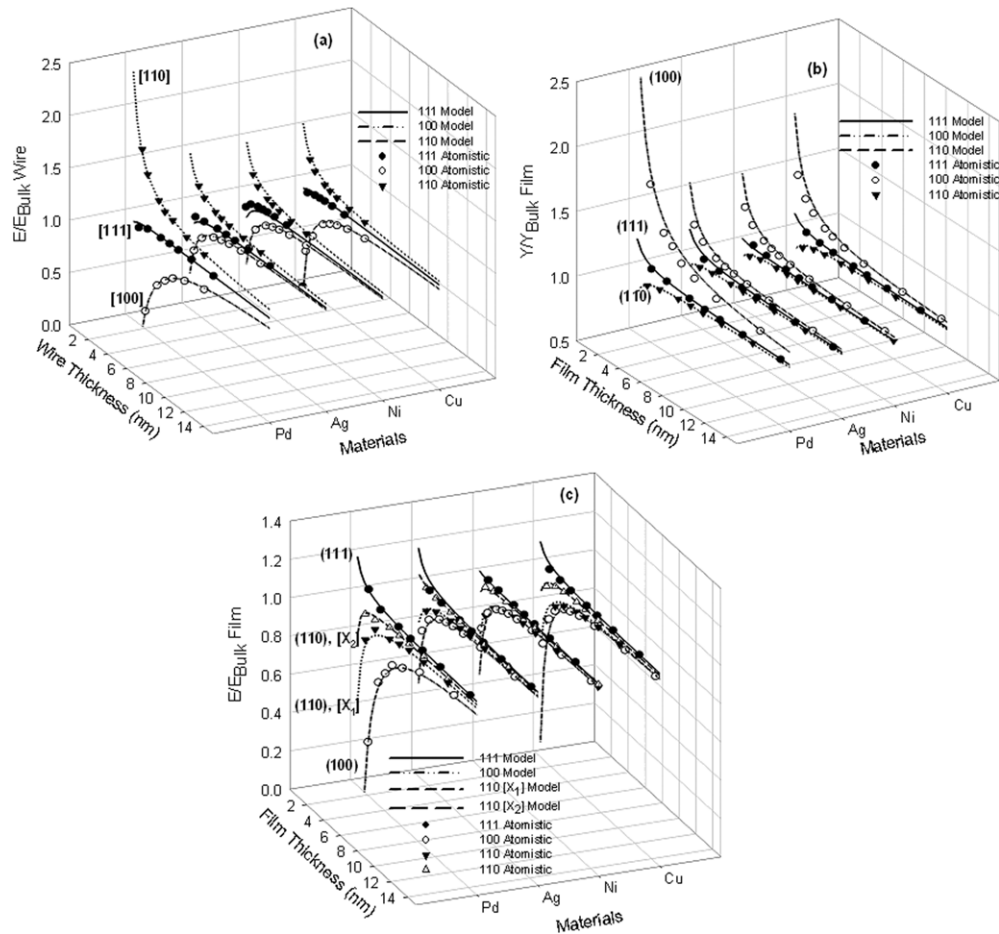


Figure 6. Elastic constants of nanowires and nanofilms for Cu, Ni, Ag and Pd; (a) Effective longitudinal elastic modulus of nanowires, (b) effective biaxial elastic modulus of nanofilms and (c) effective uniaxial elastic modulus of nanofilms, as functions of thickness for various orientations and materials calculated using the semi-analytical method (labeled as ‘atomistic’) with EAM potentials. A comparison with results obtained using the method of Dingreville and Qu [26] (labeled as ‘model’) is also shown.

properties, (iii) it is very general and applies to any interatomic potential, although an EAM potential was used in this paper in the numerical examples, and (iv) it implicitly accounts for the effects of the shape and size of the nanostructure studied. Nanostructures of different geometric shapes and sizes such as nanowires, nanofilms and nanoparticles can be studied using this method in a uniform manner without modifications to the formulation. In addition to its efficiency and simplicity, this method yields results that are in excellent agreement with those measured from experiments and predicted by other atomistic methods.

Using the method developed in this paper, the size dependence of the elastic properties of nanowires and nanofilms of Cu, Ni, Ag and Pd with [1 1 1], [1 0 0] and [1 1 0] crystallographic orientations has been investigated. The results show that the size, orientation and shape of the nanostructures influence elastic constants in different manners. Specifically, for the materials studied, decreasing the characteristic size of the nanowires from 8 to 2 nm results in decreases of the elastic modulus of up to 80% for the [1 0 0] oriented wires and up to 8% for the [1 1 1]

oriented wires and increases between 15% and 37% for the [1 1 0] oriented wires. In the case of nanofilms, as the film thickness is decreased from 8 to 2 nm, the biaxial modulus can change by up to 50%, 7% and -5% for the [1 0 0], [1 1 1] and [1 1 0] films, respectively. Among the materials in this homologous series analyzed, similar trends in elastic properties are observed, consistent with what is reported in the literature.

Acknowledgments

The authors acknowledge the financial support from the NSF through the Packaging Research Center at Georgia Tech. JQ was also supported in part by NSFC through Grant No 10228204 and by the Harbin Institute of Technology. MZ acknowledges the support from the NSF through Grant No CMS9984298 and the NSFC through Grant No 10528205. Computations were carried out at the NAVO and ASC MSRCs through AFOSR MURI No D49620-02-1-0382.

Appendix

It follows from (7)–(9) that, for the EAM potential given by (17),

$$A^{(n)} = G \left(\sum_{m \neq n} \rho(\hat{r}^{mn}) \right) + \frac{1}{2} \sum_{m \neq n} V(\hat{r}^{mn}), \quad (20)$$

$$A_{ij}^{(n)} = \left[\sum_{p \neq n} \hat{r}_j^{pn} \left(\frac{\partial G}{\partial r_i^{pn}} + \frac{1}{2} \frac{\partial V}{\partial r_i^{pn}} \right) \right]_{r^{mn} = \hat{r}^{mn}} \Big|_{(i,j)} \quad (21)$$

and

$$A_{ijkl}^{(n)} = \left[\sum_{p \neq n} \sum_{q \neq n} \hat{r}_j^{pn} \hat{r}_l^{qn} \left(\frac{\partial^2 G}{\partial r_i^{pn} \partial r_k^{qn}} + \frac{1}{2} \frac{\partial^2 V}{\partial r_i^{pn} \partial r_k^{qn}} \right) \right]_{r^{mn} = \hat{r}^{mn}} \Big|_{(i,j),(k,l)} \quad (22)$$

where

$$\frac{\partial G}{\partial r_i^{pn}} = G' \left(\sum_{m \neq n} \rho(r^{mn}) \right) \rho'(r^{pn}) \frac{r_i^{pn}}{r^{pn}}, \quad (23)$$

$$\begin{aligned} \frac{\partial^2 G}{\partial r_i^{pn} \partial r_k^{qn}} &= G'' \left(\sum_{m \neq n} \rho(r^{mn}) \right) \left[\rho'(r^{qn}) \frac{r_k^{qn}}{r^{qn}} \right] \left[\rho'(r^{pn}) \frac{r_i^{pn}}{r^{pn}} \right] \\ &+ G' \left(\sum_{m \neq n} \rho(r^{mn}) \right) \left[\rho'(r^{pn}) \left(\frac{\delta_{ik}}{r^{pn}} - \frac{r_i^{pn} r_k^{pn}}{(r^{pn})^3} \right) + \rho''(r^{pn}) \frac{r_i^{pn} r_k^{pn}}{(r^{pn})^2} \right] \delta_{pq}, \end{aligned} \quad (24)$$

$$\frac{\partial V}{\partial r_i^{pn}} = V'(r^{pn}) \frac{r_i^{pn}}{r^{pn}}, \quad (25)$$

and

$$\frac{\partial^2 V}{\partial r_i^{pn} \partial r_k^{qn}} = \left[V''(r^{pn}) \frac{r_i^{pn} r_k^{pn}}{(r^{pn})^2} + V'(r^{pn}) \left(\frac{\delta_{ik}}{r^{pn}} - \frac{r_i^{pn} r_k^{pn}}{(r^{pn})^3} \right) \right] \delta_{pq}. \quad (26)$$

In the above equations, prime and double primes on a function indicate the first and second derivatives, respectively, with respect to the argument of the function. For example, $V''(r) = d^2V/dr^2$.

References

- [1] Gleiter H 1989 Nanocrystalline materials *Prog. Mater. Sci.* **33** 223–315
- [2] Morris D G 1998 *Mechanical Behavior of Nanostructured Materials* (Endfield, NH: Trans Tech Publications, Inc.)
- [3] Diao J, Gall K and Dunn M L 2003 Surface-stress-induced phase transformation in metal nanowires *Nature Mater.* **2** 656–60
- [4] Diao J, Gall K and Dunn M L 2004 Atomistic simulation of the structure and elastic properties of gold nanowires *J. Mech. Phys. Solids* **52** 1935–62
- [5] Gryaznov V G, Kaprelov A M and Romanov A E 1989 Size effect of dislocation stability in small particles and microcrystallites *Scr. Metall.* **23** 1443–8
- [6] Kulkarni A J and Zhou M 2006 Surface-effects-dominated mechanical and thermal responses of zinc oxide nanobelts *Acta Mech. Sin.* **22** 217
- [7] Kulkarni A J, Zhou M and Ke F J 2005 Orientation and size dependence of the elastic properties of zinc oxide nanobelts *Nanotechnology* **16** 10
- [8] Liang W and Zhou M 2005 Pseudoelasticity of single crystalline Cu nanowires through reversible lattice reorientations *J. Eng. Mater. Technol.* **127** 423–33
- [9] Liang W and Zhou M 2006 Atomistic simulations reveal shape memory of fcc metal nanowires *Phys. Rev. B* **73** 115409
- [10] Kulkarni A J and Zhou M 2006 Size-effects-dominated thermal and mechanical responses of zinc oxide nanobelts *Acta Mech. Sin.* **22** 217
- [11] Kulkarni A J *et al* 2006 Novel phase transformation in ZnO nanowires under tensile loading *Phys. Rev. Lett.* **97** 105502
- [12] Miller R E and Shenoy V B 2000 Size-dependent elastic properties of nanosized structural elements *Nanotechnology* **11** 139–47
- [13] Batra I P *et al* 1986 Dimensionality and size effects in simple metals *Phys. Rev. B* **34** 8246–57
- [14] Wu Y *et al* 2004 Single-crystal metallic nanowires and metal/semiconductor nanowire heterostructures *Nature* **430** 61
- [15] Jelínek P *et al* 2003 First-principles simulations of the stretching and final breaking of Al nanowires: mechanical properties and electrical conductance *Phys. Rev. B* **68** 085403
- [16] Opitz J, Zahn P and Mertig I 2002 Ab initio calculated electronic structure of metallic nanowires and nanotubes *Phys. Rev. B* **66** 245417
- [17] Zheng J C *et al* 2002 Structural and electronic properties of Al nanowires: an ab initio pseudopotential study *Int. J. Nanosci.* **1** 159–69
- [18] Ponomareva I *et al* 2005 Structure, stability, and quantum conductivity of small diameter silicon nanowires *Phys. Rev. Lett.* **95** 265502
- [19] Wen Y H *et al* 2005 The uniaxial tensile deformation of Ni nanowire: atomic-scale computer simulations *Physica E* **27** 113–20
- [20] Wen Y H *et al* 2004 Size effects on the melting of nickel nanowires: a molecular dynamics study *Physica E* **25** 47–54
- [21] Zhang H Y *et al* 2004 Structures and properties of Ni nanowires *Phys. Lett. A* **331** 332–6
- [22] Liang H, Upmanyu M and Huang H 2005 Size-dependent elasticity of nanowires: nonlinear effects *Phys. Rev. B* **71** 241403(R)
- [23] Streitz F H, Cammarata R C and Sieradzki K 1994 Surface-stress effects on elastic properties: I. Thin metal films *Phys. Rev. B* **49** 10699
- [24] Sun C T and Zhang H 2003 Size-dependent elastic moduli of platelike nanomaterials *J. Appl. Phys.* **93** 1212–8
- [25] Zhang P *et al* 2002 The elastic modulus of single-wall carbon nanotubes: a continuum analysis incorporating interatomic potentials *Int. J. Solids Struct.* **39** 3893–906
- [26] Dingreville R, Qu J and Cherkaoui M 2005 Surface free energy and its effect on the elastic behavior of nano-size particles, wires and films *J. Mech. Phys. Solids* **53** 1827–54
- [27] Digilov R M *et al* 1976 Measurement of the surface tension of refractory metals in the solid state *Phys. Met. Metall.* **41** 68–71
- [28] Tyson W R and Miller W A 1977 Surface free energies of solid metals: estimation from liquid surface tension measurements *Surf. Sci.* **62** 267–76
- [29] Ackland G J and Finnis M W 1986 Semi-empirical calculation of solid surface tensions in body-centered cubic transition metals *Phil. Mag. A* **54** 301–15
- [30] Baskes M I 1992 Modified embedded-atom potentials for cubic materials and impurities *Phys. Rev. B* **46** 2727–42

- [31] Daw M S and Baskes M I 1983 Semiempirical, quantum mechanical calculation of hydrogen embrittlement in metals *Phys. Rev. Lett.* **50** 1285–8
- [32] Daw M S and Baskes M I 1984 Embedded-atom method: derivation and application to impurities, surfaces, and other defects in metals *Phys. Rev. B* **29** 6443–53
- [33] Mishin Y, Farkas D, Mehl M J, Papaconstantopoulos D A, Voter A F and Kress J D 2001 Structural stability and lattice defects in copper: *ab initio*, tight-binding, and embedded-atom calculations *Phys. Rev. B* **63** 224106–22
- [34] Mishin Y *et al* 1999 Interatomic potentials for monoatomic metals from experimental data and *ab initio* calculations *Phys. Rev. B* **59** 3393–407
- [35] Mishin Y *et al* 1999 Interatomic potentials for Al and Ni from experimental data and *ab initio* calculations *Mater. Res. Soc. Symp.–Proc.* **538** 535–40
- [36] Dingreville R and Qu J 2007 A semi-analytical method to compute surface elastic properties *Acta Mater.* **55** 141–7
- [37] Johnson R A 1972 Relationship between two-body interatomic potentials in a lattice model and elastic constants *Phys. Rev. B* **6** 2094–100
- [38] Oh D J and Johnson R A 1988 Simple embedded atom method model for fcc and hcp metals *J. Mater. Res.* **3** 471–8
- [39] Foiles S M, Baskes M I and Daw M S 1986 Embedded-atom-method functions for the fcc metals Cu, Ag, Au, Ni, Pd, Pt, and their alloys *Phys. Rev. B* **33** 7983–91
- [40] Haile J M 1992 *Molecular Dynamics Simulation* 2nd edn (New York: Wiley)
- [41] Chen D L and Chen T C 2005 Mechanical properties of Au nanowires under uniaxial tension with high strain-rate by molecular dynamics *Nanotechnology* **16** 2972–81
- [42] Wu H A 2006 Molecular dynamics study on mechanics of metal nanowire *Mech. Res. Commun.* **33** 9–16
- [43] Varshni Y P 1970 Temperature dependence of the elastic constants *Phys. Rev. B* **2** 3952–8
- [44] Gruber A, Gspann J and Hoffmann H 1999 Nanostructures produced by cluster beam lithography *Appl. Phys. A: Mater. Sci. Process.* **68** 197–201
- [45] Dingreville R 2007 Modeling and characterization of the elastic behavior of interfaces in nanostructured materials: from an atomistic description to a continuum approach *PhD Dissertation* Georgia Institute of Technology, Atlanta
- [46] Zhou L G and Huang H 2004 Are surfaces elastically softer or stiffer? *Appl. Phys. Lett.* **84** 1940–2
- [47] Bonnetie E 1995 Anelasticity and structural stability of nanostructured metals and compounds *Nanostruct. Mater.* **6** 639
- [48] Fougere G E *et al* 1995 Young's modulus of nanocrystalline Fe measured by nanoindentation *Mater. Sci. Eng. A* **204** 1–6
- [49] Korn D *et al* 1988 Measurements of the elastic constants and the specific heat and the entropy of grain boundaries by means of ultrasound *J. Physique (Paris)* **49** 769
- [50] Latapie A and Farkas D 2003 Effect of grain size on the elastic properties of nanocrystalline alpha-iron *Scr. Mater.* **48** 611–5
- [51] Lund A C and Schuh C A 2005 Strength asymmetry in nanocrystalline metals under multiaxial loading *Acta Mater.* **53** 3193–205
- [52] Phillpot S R, Wolf D and Gleiter H 1995 Molecular-dynamics study of the synthesis and characterization of a fully dense, three-dimensional nanocrystalline material *J. Appl. Phys.* **78** 847–61
- [53] Schiøtz J, Di Tolla F D and Jacobsen K W 1998 Softening of nanocrystalline metals at very small grain sizes *Nature* **391**
- [54] Suryanarayana C 1995 Nanocrystalline materials *Int. Mater. Rev.* **40** 41–64